RSC Advances

PAPER

Cite this: *RSC Adv.*, 2016, **6**, 111070

The role of zirconia in cobaltosic oxide catalysts for low-temperature CO oxidation

Fan Du,[a] Guisheng Wu,*[a] Dongsen Mao*[a] and Guanzhong Lu[ab]

Received 16th September 2016
Accepted 12th November 2016

DOI: 10.1039/c6ra23098a

www.rsc.org/advances

A series of Co_3O_4/ZrO_2 catalysts for low-temperature CO oxidation was prepared with different ZrO_2 loadings and different preparation methods, and then characterized by low-temperature N_2 adsorption/desorption, XRD, TEM, XPS, UV-vis, CO-TPR, CO adsorption and CO_2 desorption. The results show that ZrO_2 not only increases the specific area and decreases the crystal size of Co_3O_4 in CZ-c-20 and CZ-f-20, but also promotes production of Co^{2+} and $-O^-$, which shows the high catalytic activity for CO oxidation. The facile decomposition of carbonate and the high redox properties over ZrO_2 promote the catalytic stability for CO oxidation.

1. Introduction

Catalytic oxidation of CO has become increasingly important in the catalytic field owing to its applications in cleaning indoor air and purifying the effluent gas from various industrial sources, automobile exhausts and fuel cells. To effectively eliminate CO, many catalytic systems, such as noble catalysts (Pt, Pd, Rh, Au),[1–4] perovskite catalysts[5–7] and transition metal oxides (TMOs) catalysts,[8–12] have been employed. Among these catalysts, although supported noble metal catalysts showed high activity for CO oxidation with 100% CO conversion from 100 °C upward in excess oxygen atmospheres,[1,2,13–19] the major disadvantages, such as high cost, easy poisoning and possibility of sintering during the treatment of the exhaust gases, limit their commercial applications and finding alternative TMOs catalysts is highly desired.

Among the TMOs, Co_3O_4, as an alternative to a noble metal, exhibits high catalytic activity for low-temperature CO oxidation[20–24] owing to its advantages of low Co–O bond energy, high adsorption ability for CO, and perfect capability to activate oxygen.[25] Over the last few decades, the properties of Co_3O_4 materials with various morphologies, such as nanospheres, nanocubes, and mesoporous structures, obtained from different preparation methods have been investigated, and it has been shown that their catalytic performances strongly depend on the exposed facet as well as the morphology. The experimental and theoretical results[21,22,25,26–29] indicated that oxygen activation plays a very important role in the reaction processes on the surface of Co_3O_4 and oxygen vacancies are thought to be the key active sites for CO oxidation. Hence, it should be a useful method to increase the CO oxidation performance of Co_3O_4 by tuning the amount of surface oxygen vacancies through pretreatments under different conditions,[29] doping heteroatoms in the bulk of Co_3O_4,[21] *etc.* Unfortunately, Co_3O_4 can easily lose its catalytic activity for because its surface is very sensitive to surface carbonate species[25] and the water concentration of the feed gas, which is thought to inhibit the O_2 activation.[29,30] Therefore, further improving the catalytic stability *via* doping with heteroatoms is imperative.

To further improve the catalytic activity and stability for CO oxidation, Co_3O_4 is often supported or promoted by other oxides, such as CeO_2,[30] SiO_2,[31] TiO_2,[32] and iron oxide.[33] In recent years, Co/ZrO_2 has been found to be an active and selective catalyst for the preferential oxidation of CO[34] and cobalt supported over ZrO_2 shows much higher activity for preferential oxidation of CO than CuO or Fe_2O_3 supported over ZrO_2.[35] Zhao *et al.*[36] also found that Co_3O_4/ZrO_2 showed the higher catalytic activity for preferential oxidation of CO than other supports (CeO_2, SiO_2, Al_2O_3, and TiO_2) for it had higher cobalt dispersion and more exposed sites for CO adsorption. Xiao and co-workers[37] also found that Co_3O_4/ZrO_2 displayed higher methane combustion activity than Co_3O_4 supported over TiO_2, Al_2O_3 and MgO. By virtue of its versatile properties, such as acid, alkaline, oxidation and reducibility, ZrO_2 is widely used as a supporter of catalysts for methanol synthesis, methanol steam reforming and low-temperature catalytic CO oxidation. It not only supports and disperses the metal component, but also promotes the catalytic performance through forming strong interactions with the metal component, which can promote species spillover between the metal and the ZrO_2 as well as stabilizing the active site of the metal component by forming oxygen vacancies. In our previous work, we also found that ZrO_2 not only promoted water molecules to dissociate and form Cu^+ active sites over Cu/ZrO_2, but also accelerated the

[a]*Research Institute of Applied Catalysis, School of Chemical and Environmental Engineering, Shanghai Institute of Technology, Shanghai 201418, PR China. E-mail: gswu@sit.edu.cn; dsmao@sit.edu.cn*

[b]*Key Laboratory for Advanced Materials, Research Institute of Industrial Catalysis, East China University of Science and Technology, Shanghai 200237, PR China*

decomposition of formate and carbonate species to CO_2.[38] Furthermore, Petrik[39] found that the water molecules strongly adsorbed on the surface of ZrO_2 readily dissociate to produce H_2, while water adsorbed over Co_3O_4 is unable to decompose to H_2. By means of XPS, Sun *et al.*[40] also found that ZrO_2 could promote water molecule to dissociate, and then CoO was oxidized to Co^{2+} over Co/ZrO_2. As is well known, adsorbed water and the formed carbonate species can result in deactivation of Co_3O_4 for CO oxidation, so introduction of ZrO_2 in Co_3O_4 might be an effective method of inhibiting its deactivation.

In the present work, three types of Co_3O_4 catalysts, in which ZrO_2 was introduced by impregnation, fractionated precipitation and co-precipitation method, and different interactions were formed because of different dispersions between zirconia and Co_3O_4, were prepared for low temperature catalytic CO oxidation. We found that ZrO_2 and its introduction methods have a remarkable effect on the catalytic performance for CO oxidation. On the basis of its physicochemical properties, surface species and the adsorption ability for CO, the role of ZrO_2 in promoting Co_3O_4's catalytic activity for CO oxidation was investigated. In addition, the effect of ZrO_2 on the catalytic stability of Co_3O_4 was also discussed.

2. Experimental section

2.1 Catalyst preparation

2.1.1 Co-precipitation method. Accurately measured stoichiometric aqueous mixtures of $Co(NO_3)_2 \cdot 6H_2O$ (A.R., Sinopharm Chemical Reagent Ltd.) and $ZrOCl_2$ (A.R., Sinopharm Chemical Reagent Ltd.) as well as of an aqueous solution of Na_2CO_3 (0.5 M, A.R., Sinopharm Chemical Reagent Ltd.) were added to the precipitating reactor under vigorous stirring at 40 °C, while the pH value of the reaction medium was kept at 9. Subsequently, these reaction media were aged under stirring for 1 h at 40 °C for 1 h. After filtration and washing with de-ionized water until the filtrate was neutral, the precursor was dried at 120 °C for 12 h, and then calcined at 450 °C for 4 h. The obtained Co_3O_4/ZrO_2 samples were denoted as CZ-c-*x*, in which c represents the co-precipitation method and *x* is the % ZrO_2 mass content (the same notation is used below), and Co_3O_4 without ZrO_2 was denoted as C-c.

2.1.2 Impregnation method. 5 g of C-c powder was poured into the 50 mL aqueous solution with stoichiometric $Zr(NO_3)_4$ under vigorous stirring at 40 °C for 4 h. After drying off excess water at 60 °C, the remainder was further dried at 120 °C for 12 h and calcined at 450 °C for 4 h, and the product was denoted as CZ-i-*x*.

2.1.3 Fractionated precipitation method. An aqueous solution of $Co(NO_3)_2$ (0.5 M) and an aqueous solution of Na_2CO_3 (0.5 M) were added to the precipitating reactor under vigorous stirring at 40 °C and pH 9. Subsequently, a solution of $Zr(NO_3)_4$ and a solution of Na_2CO_3 were added under the same precipitation conditions as in Section 2.1.1. The processing procedure used for the suspension liquid was the same as that described in Section 2.1.1 and the obtained catalyst was labeled as CZ-f-*x*.

2.2 Catalytic activity testing

The catalytic activities of the prepared catalysts for CO oxidation were determined in a fixed-bed flow reactor at atmospheric pressure. 200 mg of catalyst (40–60 mesh) and 500 mg of silica sand were mixed and placed in the center of a quartz reactor (diameter 6 mm). After being pretreated in N_2 flow (30 mL min^{-1}, purity: 99.99%) at 300 °C for 1 h and then cooled down to reaction temperature, the feed gas consisting of 2% CO, 10% O_2 and 88% N_2 (30 mL min^{-1}) was passed through the catalysts. The reaction temperature was controlled by a cold trap filled with some amount of liquid nitrogen, in which different temperatures are obtained at different heights above the liquid level of the liquid nitrogen. The concentrations of CO and CO_2 in the tail gas from the reactor were analyzed on-line by a gas chromatograph (GC 2060), in which CO and CO_2 were separated by TDX-01 column, and were then converted into methane by a methane reforming furnace, then finally analyzed with a hydrogen flame ionization detector.

2.3 Characterization of the catalysts

The BET surface areas of the samples were measured by N_2 adsorption–desorption at −196 °C on a micromeritics ASAP-2020 instrument, and were calculated by the Brunauer–Emmett–Teller (BET) method. Powder X-ray diffraction (XRD) patterns were recorded on a PANalytical PW 3040/60 X'Pert Pro powder diffractometer using Cu-Kα radiation, which was operated at 40 kV and 40 mA with a scanning speed of 4° min^{-1}. The crystal size of Co_3O_4 was calculated from XRD spectra by using the Scherrer equation. High resolution transmission electron microscopy (HR-TEM) images were obtained on a Hitachi Model H-800 microscope operated at 200 kV, and the sample to be measured was first dispersed in ethanol and then collected on a copper grid covered with carbon film. After the liquid phase was evaporated, the grid was loaded into the microscope. Energy dispersive X-ray (EDX) and dot maps of the catalysts were characterized by scanning electron microscopy (type HITACHI S-4800) with an accelerating voltage of 3 kV. UV-vis diffuse reflectance spectroscopy measurements were carried out on a UV-3600 spectrometer equipped with an integration sphere. X-ray photoelectron spectra (XPS) were recorded using a JEOL JPS-9000MX with Mg Kα radiation at 10 kV and 10 mA using C_1S 284.2 eV as an internal standard. All the catalysts were pretreated for 1 h in N_2 at 300 °C before UV-vis and XPS measurements.

CO adsorption and CO_2 desorption were performed in a quartz tube reactor system equipped with a quadrupole mass spectrometer (MS, IPC 400, INFICON Co. Ltd.). 200 mg of sample (40–60 mesh) was pretreated in N_2 (purity: 99.99%) at 300 °C for 60 min then cooled down to room temperature. Subsequently, a mixture of 5% CO/N_2 was passed through the catalysts at 30 mL min^{-1} for 30 min; meanwhile the signals of CO ($m/z = 28$) and CO_2 ($m/z = 44$) were recorded using a quadrupole mass spectrometer. After that, the sample was swept with a 40 mL min^{-1} He stream (purity: 99.99%) until no CO signal was determined. Finally, the sample was heated in 40 mL min^{-1} He flow from ambient temperature to 750 °C at

a ramping rate of 10 °C min^{-1}; meanwhile, the CO and CO_2 signals were recorded.

The redox properties of the catalysts (CO-TPR) were determined in a quartz U-tube equipped with a quadrupole mass spectrometer (MS, IPC 400, INFICON Co. Ltd.). 200 mg of catalyst was pretreated in N_2 (purity: 99.99%) at 300 °C for 60 min, then cooled down to room temperature, and then exposed in the flow of 10 vol% H_2/N_2 mixture (30 mL min^{-1}). After obtaining a balanced baseline, the sample was heated from room temperature to 800 °C at a ramping rate of 10 °C min^{-1}; meanwhile the CO signal was recorded.

3. Results

3.1 Catalytic performance

To clarify the effect of ZrO_2 on the catalytic activity for CO oxidation over Co_3O_4/ZrO_2, the variation trends of catalytic activity on the ZrO_2 are presented in Fig. 1. It is clear that the ZrO_2 components brought about the remarkable influence on the catalytic activity for CO oxidation, in which the lowest temperature of complete conversion (LTCC) decreased from −50 °C to −85 °C with increasing ZrO_2 loading from 0% to 10%, maintained at −85 °C from 10% to 20% ZrO_2, increased to −45 °C with 40% ZrO_2 and sharply increased to 150 °C with 50% ZrO_2. These results illustrated that the main component being Co_3O_4 in CZ catalysts is necessary to obtain the high activity for CO oxidation. As is well known, Co_3O_4 is easy to deactivate even in the presence of trace amounts of vapor in the feed gas; accordingly, the catalytic stability at the LTCC is also shown in Fig. 1. When 3% ZrO_2 was introduced, the duration of complete conversion of CO at the LTCC decreased to 60 min relative to C-c, which should be attributed to the decrease of the reaction temperature (LTCC). Moreover, it further increased with further increased ZrO_2 loading and reached 130 min with 20% ZrO_2, then decreased to 60 min with further increase of ZrO_2. Therefore, CZ-c-20 (with 20% ZrO_2) showed the optimal catalytic performance with the dual nature of the highest catalytic activity and the highest stability.

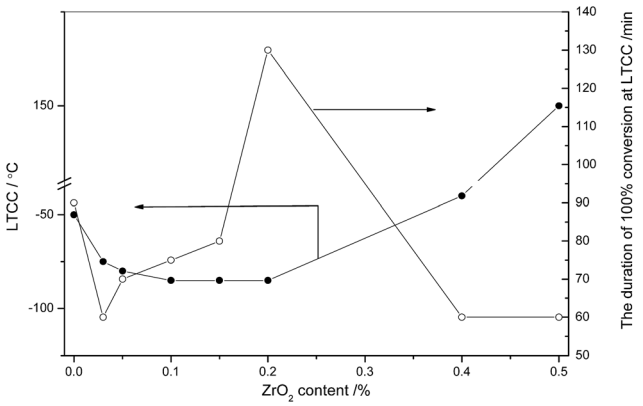

Fig. 1 Effects of ZrO_2 loading on catalytic activity for CO oxidation over Co_3O_4/ZrO_2, in which solid and hollow circles represent the lowest temperature of complete conversion (LTCC) for CO and the duration of the catalysts maintaining complete CO conversion at LTCC, respectively.

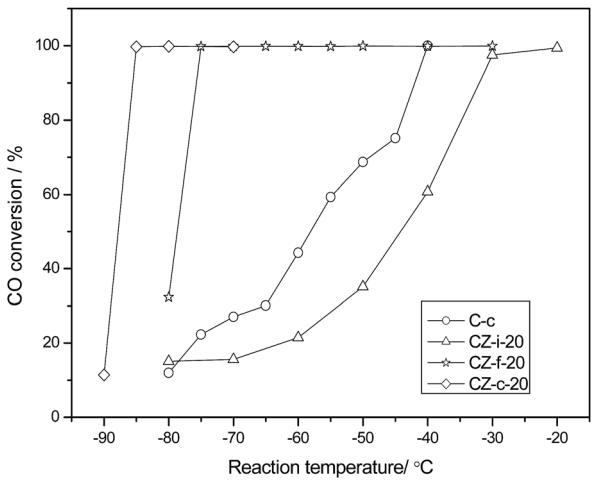

Fig. 2 The catalytic activities for CO oxidation over Co_3O_4/ZrO_2 with different preparation methods.

As shown in Fig. 2, the preparation methods have a significant influence on the performance of the catalyst for CO oxidation. Among them, CZ-c-20 exhibits the highest catalytic activity with 100% CO conversion at −85 °C while CZ-i-20 shows the lowest activity with 100% CO conversion at −20 °C. Furthermore, CZ-f-20 shows a little lower catalytic activity than CZ-c-20 with an LTCC of −75 °C, and C-c shows an LTCC of −40 °C.

The stability of the CZ catalysts with different preparation methods during the CO oxidation reaction was also investigated in on-stream operation at the LTCC and the results are displayed in Fig. 3. Among them, the catalytic stability decreased in the order of CZ-f-20 > CZ-c-20 > C-c > CZ-i-20, which is similar to the activity variation trends except for the sequence of CZ-f-20 and CZ-c-20 was reversed. In spite of the highest activity of CZ-c-20, CZ obtained from the fractionated precipitation method exhibited the highest stability with much higher activity relative to that of C-c; in contrast, impregnation of ZrO_2 over Co_3O_4 markedly lowered the activity and stability, illustrating that the physical state of ZrO_2 and interaction between Co_3O_4 and ZrO_2 could significantly affect the catalytic performance.

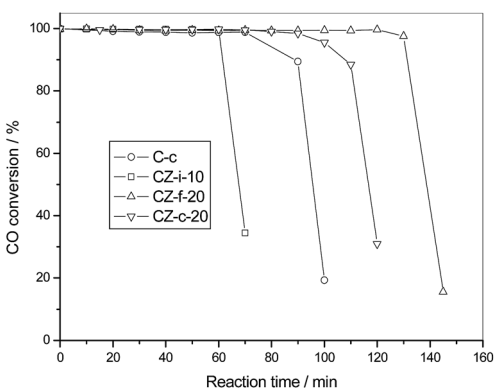

Fig. 3 Stability tests of the catalysts for CO oxidation.

Table 1 Physical properties of Co_3O_4/ZrO_2 catalysts

Sample	$S_{BET}/m^2\ g^{-1}$	Crystal size of Co_3O_4/nm
C-c	124	17.5
CZ-i-10	95	16.9
CZ-f-20	169	15.8
CZ-c-5	161	16.0
CZ-c-10	160	16.1
CZ-c-20	167	15.6
CZ-c-40	156	16.9

3.2 N_2 adsorption–desorption and XRD

With the help of low-temperature N_2 adsorption, the BET surface areas (S_{BET}) of the catalysts were determined to clarify the effect of ZrO_2 on the specific area of Co_3O_4. As shown in Table 1, pure Co_3O_4 exhibited the largest surface area of 124 $m^2\ g^{-1}$, which could account for the high activity of C-c. With the introduction of ZrO_2, the specific areas of the catalysts showed a different change; for example, that of CZ-i-10 dropped to 95 $m^2\ g^{-1}$, while those of CZ-f-20 and CZ-c-20 increased to 169 and 167 $m^2\ g^{-1}$, respectively. Combined with the variation trend of catalytic activities, it is clear that introduction of ZrO_2 with co-precipitation or fractionated precipitation can lead to the increase of the specific area of Co_3O_4 and then promote the catalytic activity, but doping ZrO_2 with impregnation methods can lower the catalytic activity due to the decrease of the specific area. As shown in Fig. 4, the XRD patterns of all catalysts exhibited the characteristic diffraction peaks of the cubic spinel structure Co_3O_4 (JCPDS card 43-1003), but were absent of any peaks of ZrO_2, illustrating that ZrO_2 is in the highly dispersed state or amorphous state. Moreover, the crystallite sizes of Co_3O_4, which were calculated by Scherrer's equation[41] and are shown in Table 1, show that the crystal size of cobaltosic oxide decreases in the order of C-c < CZ-i-10 < CZ-f-20 < CZ-c-20, illustrating that ZrO_2 introduced through co-precipitation or fractionated precipitation method remarkably promotes the dispersion of Co_3O_4.

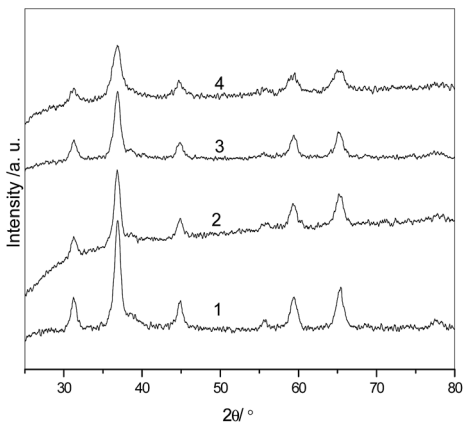

Fig. 4 XRD spectra of C-c (1), CZ-i-10 (2), CZ-f-20 (3) and CZ-c-20 (4).

3.3 Transmission electron microscopy (TEM)

As shown in Fig. 5, the morphologies of C-c, CZ-f-20 and CZ-c-20 observed using transmission electron microscopy (TEM) reveal that the particles composing all the catalysts are ellipsoidal and C-c displays the distribution of particles of size 15–19 nm, which is reduced to 14–16 nm with the introduction of ZrO_2 and is consistent with the results of crystal size from the Scherrer formula from the XRD data. It is difficult to distinguish Co_3O_4 from ZrO_2 in the TEM images, but the (111) planes with spacing of 0.462 nm present in all samples, illustrating that the ZrO_2 promoter does not obviously change the morphology of Co_3O_4.

3.4 EDX analysis

The EDX analyses of prepared samples are shown in Fig. 6 to illustrate the elements dispersion and distribution on the surface of the catalysts. As shown in Fig. 6, the component distributions of both samples are uniform in spite of the different catalyst preparation methods. Compared with the ratios of components, it is shown that the contents of Zr and O are higher on the surface of CZ-f-20 than those on the surface of CZ-c-20, illustrating that the subsequent precipitation of the Zr component in the process of the fractionated precipitation method can cause enrichment of Zr and O on the surface of the CZ catalysts.

3.5 X-ray photoelectron spectroscopy (XPS)

As we all know, the XPS spectra of CoO_x samples consist of two main peaks at about 780 eV for Co $2p_{3/2}$ and at 795.5 eV for Co $2p_{1/2}$. Although the binding energies of Co $2p_{3/2}$ and Co $2p_{1/2}$ of Co^{2+} are relatively vicinal, the Co^{2+} can be distinguished by the shake-up satellite peaks at ~787.0 and 804.0 eV, arising from the presence of unpaired electrons in the 3d orbital of Co^{2+}. Unlike the Co^{2+} compounds, Co^{3+} is almost always absent from unpaired electrons and is in a low spin state in the octahedron

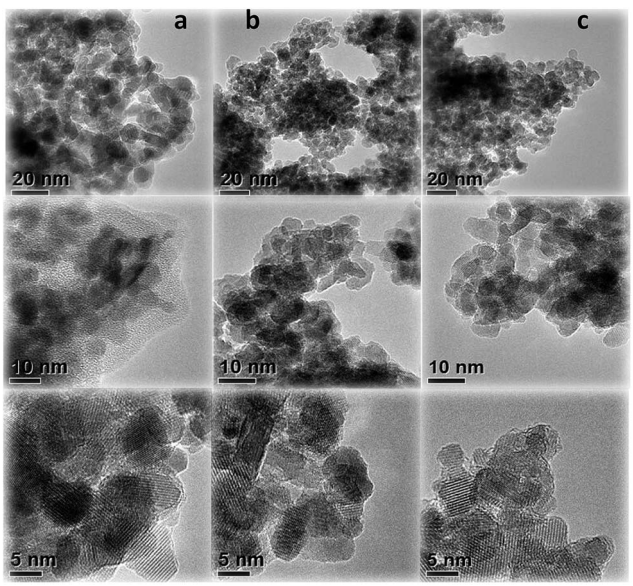

Fig. 5 TEM images of C-c (a), CZ-f-20 (b) and ZC-c-20 (c).

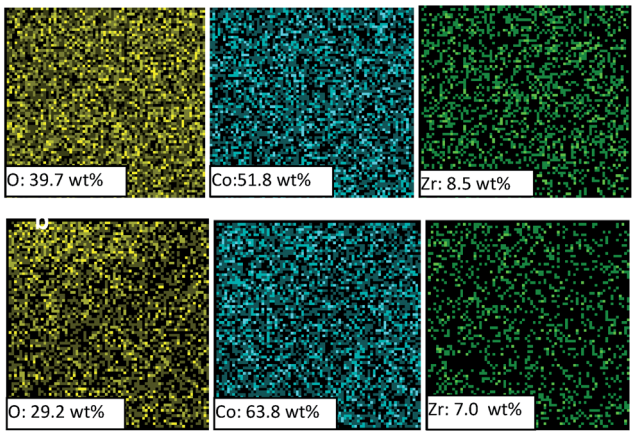

Fig. 6 EDX analysis of, CZ-f-20 (a) and ZC-c-20 (b).

coordination, therefore the shake-up satellite peaks are not observed owing to no energy transfer to an unpaired electron.[33] As shown in Fig. 7(a), the satellite peaks at 787 and 804 eV increase in the sequence of C-c < CZ-f-20 < CZ-c-20, illustrating that introduction of ZrO_2 can increase the content of Co^{2+}.

The O 1s XPS spectra shown in Fig. 7(b) consist of a main peak at 529.9 eV with a shoulder peak at 531.1 eV attributed to

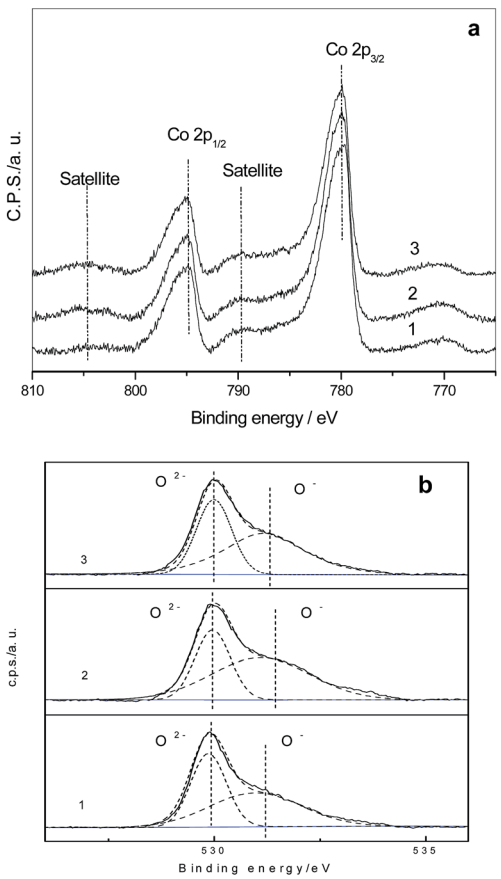

Fig. 7 The Co 2p (a) and O 1s (b) XPS spectra of C-c (1), CZ-f-20 (2) and CZ-c-20 (3).

Table 2 Curve-fitting results from XPS data on the O 1s binding energies (BE), and the relative amount (%) of the oxygen-containing species in various samples

Catalyst	C-c	CZ-f-20	CZ-c-20
OI[a]	529.86 (45%)	529.96 (35.4%)	529.99 (42.6%)
OII[a]	530.97 (55%)	531.09 (64.6%)	531.17 (57.4%)

[a] The position of OI or OII based on which the curve of OI/OII was fitted and the relative amount of OI or OII, which is shown in parentheses and was the ratio of the intensity of the OI or OII peak to that of the total O 1s peak.

two types of oxygen species. In general, the peak at ~529.9 eV is associated with lattice oxygen species ($-O^{2-}-$, denoted as OI) and that at 531.1 may be ascribed to oxygen species (denoted as OII) in hydroxyl groups or $-O^-$.[42,43] Deconvolution of the original O 1s features was carried out based on the position at about 529.9 and 531.1 eV and the peak positions and their relative contents are summarized in Table 2. It is clear that the ratio of OII : OI decreases in the sequence of C-c < CZ-c-20 < CZ-f-20. It is well known that ZrO_2 can promote the dissociative adsorption of water to form the hydroxyl over the catalysts, which illustrates the increase of OII species.

3.6 UV-vis diffuse reflection spectroscopy

The catalysts were also investigated by UV-visible reflection spectroscopy (UV-vis), which is shown in Fig. 8(a). C-c shows two distinct absorption bands centered at about 430 and 735 nm, which were assigned to the ligand to metal charge transfer (LMCT) events, such as $O^{2-} \rightarrow Co^{2+}$ for the first adsorptions (λ < 500 nm) and $O_2^- \rightarrow Co^{3+}$ for the second adsorptions (λ > 750 nm).[44,45] With the introduction of ZrO_2, the absorption edge shifted to lower energy longer wave length, with CZ-f-20 and CZ-c-20 centering at about 399 and 690 nm and CZ-i-10 at 356 and 653 nm. Furthermore, the absorption band gap (E_g) of the catalysts could be estimated by the following relation: $(Ahv)^2 = B(hv - E_g)$,[45,46] in which hv is the photon energy (eV), A is the optical density, B is a constant, and E_g is the band gap described above. The plot of $(Ahv)^2$ *vs.* hv is drawn to calculate the band gap by extrapolating the linear region in the plot of $(\alpha hv)^2$ *vs.* hv, which is shown in Fig. 8(b). The C-c exhibits two E_g values of 1.37 and 2.62 eV which are ascribed to the E_g of the $O_2^- \rightarrow Co^{3+}$ (E_{g1}) and $O^{2-} \rightarrow Co^{2+}$ (E_{g2}) charge transfer processes, respectively, and are close to the values obtained from Co_3O_4 nanoparticles.[46] Introduction of ZrO_2 components in Co_3O_4 leads to the decrease of both of E_{g1} and E_{g2}; for example, the E_g of CZ-i-10 are 1.33 and 2.22 eV, those of CZ-f-20 and those of CZ-c-20 are 1.33 and 2.4 eV.

3.7 CO adsorption and CO_2-TPD

In order to monitor the responsivity of the surface of the catalysts to CO, the adsorption of CO was carried out and the results are shown in Fig. 9(a). When CO was introduced through the catalysts, some amount of CO was adsorbed with a small amount of CO_2 released. With the lengthening of the adsorption

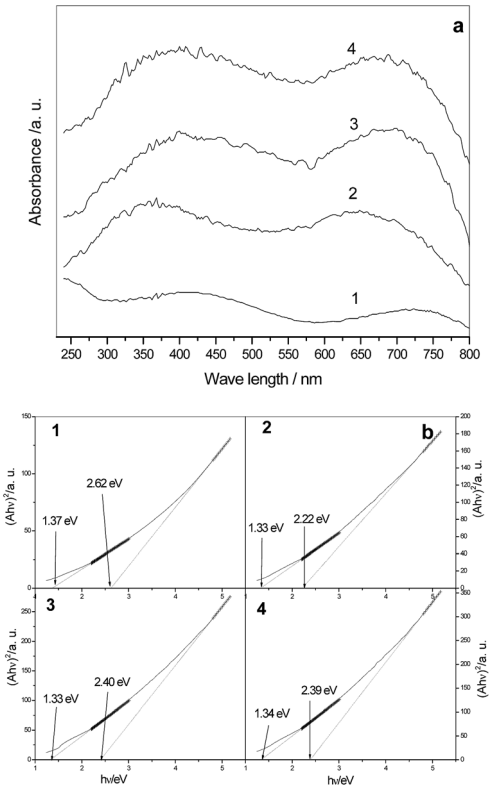

Fig. 8 UV-vis spectra (a) of C-c (1), CZ-i-10 (2), CZ-f-20 (3) and CZ-c-20 (4) and the plot of $(Ah\nu)^2$ *versus* $h\nu$ (b) for C-c (1), CZ-i-10 (2), CZ-f-20 (3) and CZ-c-20 (4).

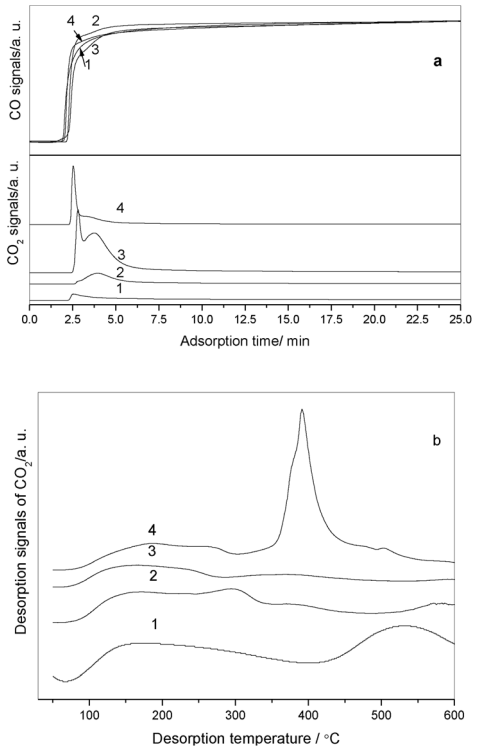

Fig. 9 CO adsorption profiles (a) of C-c (1), CZ-i-10 (2), CZ-f-20 (3) and CZ-c-20 (4) and TPD profiles of CO_2 (b) after CO adsorption at ambient temperature for 30 min over C-c (1), CZ-i-10 (2), CZ-f-20 (3) and CZ-c-20 (4).

time, CO adsorption gradually reaches saturation state and the CO adsorption signal becomes a horizontal line. Comparing with CO adsorption signals over the different catalysts in Fig. 9(a), it is clear that the amount of CO adsorption increases in the sequence of CZ-i-10 < CZ-c-20 < C-c < CZ-f-20 and the amount of released CO_2 increased in the order of C-c < CZ-i-10 < CZ-c-20 < CZ-f-20. Furthermore, it is illustrated that the ZrO_2 can promote the CO_2 to release and C-c shows the high amount of CO adsorption despite the lower amount of CO_2.

After CO adsorption saturation, CO_2-TPD was carried out and is shown in Fig. 9(b). It is shown that all catalysts exhibit a broad CO_2 desorption peak at 70–350 °C, and its intensity over CZ-f-20 and CZ-c-20 is much larger than that over C-c and CZ. In addition, C-c shows a very strong desorption peak centered at about 400 °C, which illustrates that carbonate species over it are stable and decomposed at higher temperature and also accounts for the large amount of CO adsorption with less CO_2 release.

3.8 Redox properties

It is well known that the redox cycles are repeated on the surface of catalysts, hence the redox properties of a catalyst are a key factor to illustrate the catalytic activity and stability for CO oxidation. As shown in Fig. 10, no evident reduction peaks are observed over C-c in the first CO-TPR, whereas introduction of zirconia can remarkably promote reduction of cobalt, in which the intensity of the reduction peak increases in the sequence of CZ-i-10 < CZ-f-20 < CZ-c-20. After the first TPR, the catalysts were oxidized at ambient temperature and were used for the second TPR. The results of the second TPR demonstrate that all samples displayed reduction peaks that were shifted to a lower temperature position than that of the first TPR. Among them, CZ-c-20 shows the strongest reduction peak whereas CZ-i-10 has the weakest peak, illustrating that the redox properties of Cz-c-20 and CZ-i-10 are the highest and the lowest, respectively, which is also in agreement with the results of catalytic activity for CO oxidation.

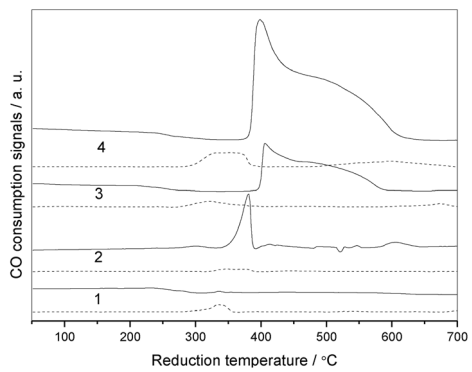

Fig. 10 CO-TPR profiles of C-c (1), CZ-i-10 (2), CZ-f-20 (3) and CZ-c-20 (4), in which the solid and dashed lines are the profiles of the first and the second TPR, respectively.

4. Discussion

ZrO_2 is widely used as a supporter or promoter in many reactions, such as methanol synthesis, methanol steam reforming, and Fischer–Tropsch (F–T) synthesis, in which ZrO_2 not only serves as the supporter to improve the dispersion of the active site and the specific surface area of the catalysts, but also to promote the electron interaction and species spillover between mental and zirconia. Chen *et al.*[46] found that the increase of the Co/Zr ratio in Co/ZrO_2 prepared by coprecipitation method can promote the reduction of cobalt species and then enhance the activity for F–T synthesis. In previous work, we also found that the interaction between copper and zirconia had a remarkable effect on the catalytic performance for methanol synthesis[47] or methanol steam reforming;[48] moreover, enrichment of zirconia on the surface of the catalysts is propitious to promote the catalytic activity.[48,49] As regards CO oxidation, ZrO_2 could reinforce the cobalt oxide and support interaction, promote the redox properties of spinel Co_3O_4, and then promote the catalytic activity for CO preferential oxidation.[35–37]

To clarify the role of ZrO_2 in Co_3O_4, the performance of Co_3O_4/ZrO_2 prepared with different Co/Zr ratios *via* co-precipitation method was investigated at first. As we expected, introducing the zirconia in Co_3O_4 can enlarge the surface area and hinder the aggregation of the Co_3O_4 crystal grains. However, the change in the trend of catalytic activity is not in agreement with that of the specific areas, illustrating that factors other than the specific area and crystal size should be taken into account. When the loadings of ZrO_2 go beyond 20%, the LTCC of CZ-40 increases in spite of further increase of the specific area. Furthermore, CZ-c-50 shows an LTCC of 150 °C. These results illustrate that the major component of the catalyst must be Co_3O_4 to ensure the high activity for CO oxidation. Zhao *et al.*[36] suggested that using ZrO_2 as a supporter can promote the formation of Co_3O_4, which is considered as the active site. Because Co_3O_4 is present over Co/ZrO_2 but is absent over Co/TiO_2, the former shows more activity for methane combustion than the latter.[38] When ZrO_2 loading is high, it can overlay over Co_3O_4 to hinder adsorption of the reactant on Co_3O_4, hence the catalytic activity is suppressed.

To further illustrate the effect of the ZrO_2 promoter, ZrO_2 was introduced by different methods of impregnation, fractionated precipitation and co-precipitation, in which impregnation can produce a weak interaction between cobalt and zirconia, and in contrast cobalt oxide and zirconia with fractionated precipitation or co-precipitation are well dispersed among each other except that ZrO_2 is specifically enriched on the surface of CZ-f-20 because of the latest precipitation process of zirconium species. Based on the catalytic activity results, it is clear that CZ-i-10 shows the lowest catalytic activity because the majority of the surface of the Co_3O_4 is covered by zirconia. Both CZ-f-20 and CZ-c-20 show much higher catalytic activity owing to the Co_3O_4 components being well dispersed and the surface of Co_3O_4 is well exposed, which is evidenced by the results of XRD, TEM and EDX. From the EDX data, it is clear that the components of O and Zr are enriched on surface of CZ-f-20, which can cause a decrease in the exposed surface of Co_3O_4 and lower catalytic activity for CO oxidation than that of CZ-c-20.

With respect to the active site of Co_3O_4, it is still debatable. For example, Xie *et al.*[24] proposed that the Co^{3+} species over Co_3O_4 nanorods should account for its perfect catalytic performance because the predominant exposed surface is (110) facets, while Pollard *et al.*[49] believe that Co^{2+} is the active site because Co_3O_4 with a low Co^{2+} : Co^{3+} ratio of approximately 1 : 4 produced by calcination at 300 °C in air shows 20% lower activity than that with a higher Co^{2+} : Co^{3+} ratio obtained by calcination at 200 °C. Furthermore, the oxidation of CO over Co_3O_4 has been proposed to follow the redox cycle mechanism, that is, the lattice oxygen on the surface of Co_3O_4 is reduced by adsorbed CO on a cobalt site to produce CO_2 with the formation of an oxygen vacancy. Subsequently, the oxygen vacancy is healed by oxidation of molecular oxygen in the feed gas to ensure the recommencement of the new redox cycle. Based on this mechanism, Sadykov and co-workers[50] proposed that the weakly bound oxygen species over Co_3O_4 induced by pretreatment in He at 350 °C should confer the high catalytic activity for CO oxidation. Yu and co-workers[28] also found that pretreatment of Co_3O_4 in inert gases also promotes the formation of surface oxygen vacancies, which has the strong adsorption ability to O_2 and then promote the catalytic for CO oxidation. In this case, all the catalysts are pretreated at 450 °C in N_2 atmosphere to enrich those active sites.

Based on the above views, the evolution of the active site is proposed as follows. As shown in Scheme 1, with the increase of the pretreatment temperature in the inert gas, the $-O^{2-}-$ bonded with Co^{3+} in octahedral coordination is broken by oxidation scission to produce $-O^-$ and Co^{2+}-v in the octahedral site, in which v denotes an oxygen vacancy. CO adsorbed on the Co^{2+}-v can be oxidized by the adjacent $-O^-$ to produce CO and Co^{2+}, moreover, an oxygen molecule can be also adsorbed on the Co^{2+}-v site to produce $-O^-$ or O^{2-} and Co^{3+}. With the help of O_2-TPD, Yu[28] proposed that O_2 adsorbed on the surface of Co_3O_4 evolves through the process of $O_2 \rightarrow O_2^- \rightarrow 2O^- \rightarrow 2O^{2-}$, hence it is reasonable that the process of O^{2-} to O^- of Co_3O_4 occurs in the anoxic atmosphere. In addition, using UV-vis, Gómez and coworkers[34] found that the shoulder at around 490 nm in the absorption bands, which is ascribed to Co^{2+} in the octahedral coordination, further certifying the rationality of

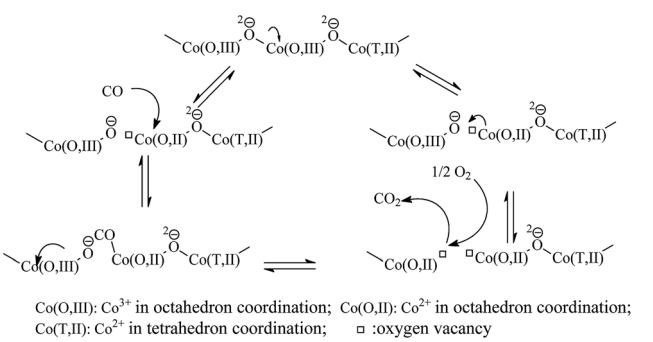

Scheme 1 The proposed evolution of the active site in CO oxidation process.

the above mechanism. In addition, we also believe that Co^{2+}-v should be the active sites for molecular CO or O_2. Based on the view of coordination chemistry, Co^{2+} not only provides the vacancy to adsorb CO or O_2, but also a low value of Co^{2+} is propitious to the feedback of the electron in its d-orbital to the antibonding orbital of CO, the 2π orbital, or that of O_2, the $1\pi_g$ orbital, hence the bond strength of C–O or O–O is weakened, as is further evidenced by the fact that the stretching-vibration wavenumber of CO bonding with Co^{2+} is 30–50 cm^{-1} lower than that with Co^{3+}.[51] Unfortunately, in the UV-vis spectra herein, the region near 490 nm is the overlay of absorption bands ascribed to the LMCT of $O^{2-} \rightarrow Co^{2+}$ and $O_2^- \rightarrow Co^{3+}$, and then the evident absorption band of Co^{2+} in the octahedral coordination is hardly identified. However, with the introduction of ZrO_2, both E_{g1} and E_{g2} decrease, illustrating that ZrO_2 can promote the process of Co^{3+}–O^{2-} to Co^{2+}-v and O^-–, which is further evidenced by the XPS results, which shows that ZrO_2 can lead to the increase of Co^{2+} and oxygen species, except for O^{2-}. Yu[28] also proposed that the O^- species can promote adsorbed CO to be oxidized to produce CO_2, which is further evidenced in CO adsorption, in which the ZrO_2 promoter can accelerate the release of CO_2. The redox properties of catalysts with the help of CO-TPR illustrate that ZrO_2 can promote the redox capacity of Co_3O_4, further illustrating the electron transmission between the oxygen species and the cobalt ions because of the introduction of ZrO_2. Relative to C-c, CZ-f-20 and CZ-c-20 show lower E_{g1} and E_{g2} in UV-vis, high amounts of Co^{2+} and OII species in XPS, and much easier redox properties, hence display much higher catalytic activity for CO oxidation.

It is well known that the main shortcoming of Co_3O_4, which limits its wider use, is its low stability. In general, the surface carbonate species were considered as one possible reason for the deactivation of CO oxidation over Co_3O_4,[25,27–30] which could cause the surface reconstruction[31] and local change of oxidation state.[51] The results of theoretical calculation also confirmed that surface carbonate species tightly occupied on the active sites of Co_3O_4 inhibit the process of CO oxidation.[52] The stability of the CZ catalysts shows the same trend whereby the catalytic activities of all catalysts dramatically dropped after a certain time on stream, illustrating that accumulation of carbonate can lead to the catalyst deactivation. From the TPD of CO_2, it is clear that a large amount of CO_2 was desorbed at around 400 °C, illustrating that the stable carbonate species formed over C-c; therefore, it is easy to lose catalytic activity. As discussed above, ZrO_2 can enrich $-O^-$ species, which can promote CO immediate oxidation to release CO_2 and then inhibit to form the stable carbonate over Co_3O_4; therefore, the stability of CZ-f-20 and CZ-c-20 is improved remarkably. Because of the weak interaction between ZrO_2 and Co_3O_4 as well as less exposed surface of Co_3O_4 induced by impregnation of zirconium species, CZ-i-10 shows the lowest catalytic activity and stability. In addition, a trace amount of water in the feed can cause deactivation of Co_3O_4, which originated from the fact that most of the active sites of Co_3O_4 are covered by H_2O. Although the role of water in CO oxidation over Co_3O_4 is not investigated in this work, according to the literature, ZrO_2 has much stronger adsorption ability for water than Co_3O_4, furthermore, adsorbed water over ZrO_2 can easily decompose to H_2 (ref. 40) and surface oxygen species. These findings further illustrate that ZrO_2 can promote the catalytic stability for CO oxidation.

5. Conclusions

A series of Co_3O_4/ZrO_2 was prepared with different ZrO_2 loadings and different preparation methods. CZ-c-20 showed the highest activity and stability, but the activity drops with further increase of ZrO_2 content. Compared with the catalytic performance with different preparation methods, CZ-c-20 shows the highest activity and CZ-f-20 exhibits the optimum stability, but CZ-i-10 shows the lowest activity and stability. The characterization results show that ZrO_2 increases the specific area and decreases the crystal size of Co_3O_4 in CZ-c-20 and CZ-f-20 because of the good dispersion of ZrO_2 and Co_3O_4. On the other hand, ZrO_2 can promote the production of Co^{2+} and $-O^-$ over CZ catalysts and then promote the catalytic activity for CO oxidation. Moreover, ZrO_2 can also promote adsorbed carbonate to decompose to CO_2, further enhancing the redox properties of Co_3O_4, hence promoting the catalytic stability.

Acknowledgements

Financial support from the National Science Foundation of China (Grant No. 20503005), Shanghai Leading Academic Discipline Project (P1501) and the program of Shanghai Municipal Education Commission, China are gratefully acknowledged.

Notes and references

1 X. Zhang, E. Long, Y. Li, J. Guo, L. Zhang, M. Gong, M. Wang and Y. Chen, *J. Nat. Gas Chem.*, 2009, **18**, 139–144.
2 N. Yamaguchi, N. Kamiuchi, H. Muroyama, T. Matsui and K. Eguchi, *Catal. Today*, 2011, **164**, 169–175.
3 S. Y. Christou, S. Garcia-Rodriguez, J. L. G. Fierro and A. M. Efstathiou, *Appl. Catal., B*, 2012, **111–112**, 233–245.
4 I. H. Son, A. M. Lane and D. T. Johnson, *J. Power Sources*, 2003, **124**, 415–419.
5 C. A. Chagas, F. S. Toniolo, R. Newton, S. H. Magalhães and M. Schmal, *Int. J. Hydrogen Energy*, 2012, **37**, 5022–5031.
6 B. Seyfi, M. Baghalha and H. Kazemian, *Chem. Eng. J.*, 2009, **148**, 306–311.
7 H. Taguchi, S. Yamasaki, A. Itadani, M. Yosinaga and K. Hirota, *Catal. Commun.*, 2008, **9**, 1913–1915.
8 S. A. C. Carabineiro, B. F. Machado, R. R. Bacsab, P. Serpb and G. DrăFigueiredo, *J. Catal.*, 2010, **273**, 191.
9 S. Y. Li, G. Liu, H. L. Lian, M. J. Jia, G. M. Zhao, D. Z. Jiang and W. X. Zhang, *Catal. Commun.*, 2008, **9**, 1045–1049.
10 M. Haruta, T. Kobayashi and N. Yamada, *Chem. Lett.*, 1987, **16**, 405–408.
11 M. S. Chen and D. W. Goodman, *Science*, 2004, **306**, 252–255.
12 B. T. Qiao, L. Q. Liu, J. Zhang and Y. Q. Deng, *J. Catal.*, 2009, **261**, 241–244.
13 B. K. Min and C. M. Friend, *Chem. Rev.*, 2007, **107**, 2709–2724.

14 N. Imanaka, T. Masui, H. Imadzu and K. Yasuda, *Chem. Commun.*, 2011, **47**, 11032–11034.
15 S. Carrettin, P. Concepción, A. Corma, J. M. López Nieto and V. F. Puntes, *Angew. Chem., Int. Ed.*, 2004, **43**, 2538–2540.
16 M. Comotti, W. C. Li, B. Spliethoff and F. Schüth, *J. Am. Chem. Soc.*, 2006, **128**, 917–924.
17 L. M. Liu, B. McAllister, H. Q. Ye and P. Hu, *J. Am. Chem. Soc.*, 2006, **128**, 4017–4022.
18 J. Gong and C. B. Mullins, *J. Am. Chem. Soc.*, 2008, **130**, 16458–16459.
19 A. A. Herzing, C. J. Kiely, A. F. Carley, P. Landon and G. J. Hutchings, *Science*, 2008, **321**, 1331–1335.
20 Y. Lou, L. Wang, Y. H. Zhang, Z. Y. Zhao, Z. G. Zhang, G. Z. Lu and Y. Guo, *Catal. Today*, 2011, **175**, 610–614.
21 D. A. H. Cunningham, T. Kobayashi, N. Kamijo and M. Haruta, *Catal. Lett.*, 1994, **25**, 257–264.
22 Y. Z. Wang, Y. X. Zhao, C. G. Gao and D. S. Liu, *Catal. Lett.*, 2007, **116**, 136–142.
23 P. Thormählen, M. Skoglundh, E. Fridell and B. Andersson, *J. Catal.*, 1999, **188**, 300–310.
24 X. W. Xie, Y. Li, Z. Q. Liu, M. Haruta and W. J. Shen, *Nature*, 2009, **458**, 746–749.
25 X. F. Tang, J. H. Li and J. M. Hao, *Mater. Res. Bull.*, 2008, **43**, 2912–2918.
26 J. Jansson, A. E. C. Palmqvist, E. Fridell, M. Skoglundh, L. Österlund, P. Thormählen and V. Langer, *J. Catal.*, 2002, **211**, 387–397.
27 J. Jansson, *J. Catal.*, 2000, **194**, 55–60.
28 Y. B. Yu, T. Takei, H. Ohashi, H. He, X. L. Zhang and M. Haruta, *J. Catal.*, 2009, **267**, 121–128.
29 H. F. Wang, R. Kavanagh, Y. L. Guo, Y. Guo, G. Z. Lu and P. Hu, *Angew. Chem., Int. Ed.*, 2011, **51**, 6657.
30 J. Li, G. Lu, G. Wu, D. Mao, Y. Wang and Y. Guo, *Catal. Sci. Technol.*, 2012, **2**, 1865–1871.
31 C. Lin, Y. Guo and J. Vela, *ACS Catal.*, 2015, **5**, 1037–1044.
32 J. Li, G. Lu, G. Wu, D. Mao, Y. Guo, Y. Wang and Y. Guo, *Catal. Sci. Technol.*, 2014, **4**, 1268–1275.
33 J. Li, G. Lu, G. Wu, D. Mao, Y. Guo, Y. Wang and Y. Guo, *RSC Adv.*, 2013, **3**, 12409–12416.
34 L. E. Gómez, I. S. Tiscornia, A. V. Boix and E. E. Miró, *Appl. Catal., A*, 2011, **401**, 124.
35 A. Firsova, T. Khomenko, O. Sil'chenkova and V. Korchak, *Kinet. Catal.*, 2010, **51**, 299–311.
36 Z. Zhao, M. M. Yung and U. S. Ozkan, *Catal. Commun.*, 2008, **9**, 1465–1471.
37 T. Xiao, S. Ji, H. Wang, K. S. Coleman and M. L. H. Green, *J. Mol. Catal. A: Chem.*, 2001, **175**, 111–123.
38 J. Zhou, Y. Zhang, G. Wu, D. Mao and G. Lu, *RSC Adv.*, 2016, **6**, 30176–30183.
39 N. G. Petrik, A. B. Alexandrov and A. I. Vall, *J. Phys. Chem. B*, 2001, **105**, 5935–5944.
40 J. Sun, A. M. Karim, D. Mei, M. Engelhard, X. Bao and Y. Wang, *Appl. Catal., B*, 2015, **162**, 141–148.
41 A. Patterson, *Phys. Rev.*, 1939, **56**, 978.
42 Q. Liu, L. C. Wang, M. Chen, Y. Cao, H. Y. He and K. N. Fan, *J. Catal.*, 2009, **263**, 104–113.
43 S. G. Christoskova, M. Stoyanova, M. Georgieva and D. Mehandjier, *Mater. Chem. Phys.*, 1999, **60**, 39–43.
44 F. Gu, C. Li, Y. Hu and L. Zhang, *J. Cryst. Growth*, 2007, **304**, 369–373.
45 Z. Y. Li, P. T. M. Bui, D.-H. Kwak, M. S. Akhtar and O.-B. Yang, *Ceram. Int.*, 2016, **42**, 1879–1885.
46 J. G. Chen and Y. H. Sun, *Stud. Surf. Sci. Catal.*, 2004, **147**, 277–282.
47 G. Wu, Y. Sun, Y. Li, H. Jiao, H. Xiang and Y. Xu, *J. Mol. Struct.: THEOCHEM*, 2003, **626**, 287–293.
48 G. Wu, D. Mao, G. Lu, Y. Cao and K. Fan, *Catal. Lett.*, 2009, **130**, 177–184.
49 M. J. Pollard, B. A. Weinstock, T. E. Bitterwolf, P. R. Griffths, A. P. Newbery and J. B. Paine, *J. Catal.*, 2008, **254**, 218–225.
50 V. A. Sadykov, S. F. Tikhov, S. V. Tsybulya, G. N. Kryukova, S. A. Veniaminov, V. N. Kolomiichuk, N. N. Bulgakov, E. A. Paukshtis, V. P. Ivanov, S. V. Koshcheev, V. I. Zaikovskii, L. A. Isupova and L. B. Burgina, *J. Mol. Catal. A: Chem.*, 2000, **158**, 361–365.
51 H. Tüysüz, M. Comotti and F. Schüth, *Chem. Commun.*, 2008, 4022–4024.
52 S. Kunz, F. F. Schweinberger, V. Habibpour, M. Röttgen, C. Harding, M. Arenz and U. Heiz, *J. Phys. Chem. C*, 2010, **114**, 1651–1654.